Inorganic Chemistry
Article

Inorg. Chem. **2009**, *48*, 7787–7793 **7787**
DOI: 10.1021/ic900724f

Displacement Kinetics of η^2-Bound Furan and 2,3-Dihydrofuran from Mn and Cr Centers: Evidence for the Partial Dearomatization of the Furan Ligand

Jeremy R. Andreatta,[†] G. Benjamin Cieslinski,[‡] Madeeha Batool,[§] Xue-Zhong Sun,[§] Michael W. George,[§] Edward N. Brothers,[‡] Donald J. Darensbourg,*[,†] and Ashfaq A. Bengali*[,‡]

[†]*Department of Chemistry, Texas A&M University, College Station, Texas 77843-3255,* [‡]*Department of Chemistry, Texas A&M University at Qatar, Doha, Qatar, and* [§]*School of Chemistry, University of Nottingham, University Park, Nottingham, NG7 2RD, U.K.*

Received April 14, 2009

The displacement of η^2-coordinated ligands from the photolytically generated $CpMn(CO)_2L$ and $BzCr(CO)_2L$ [Cp = η^5-C_5H_5, Bz = η^6-C_6H_6, L = 2,3-dihydrofuran (DHF), furan] complexes by pyridine has been studied. The displacement reactions span a wide range of time scales from microseconds to hours and were studied using a range of time-resolved IR spectroscopic techniques. The substitution reactions follow a dissociative pathway and the measured activation enthalpies provide an estimate for the strength of the metal−(η^2-furan) and metal−(η^2-DHF) interactions. In these complexes, the Cr center binds both ligands weaker than the Mn center. There is a ∼6−10 kcal/mol difference in the binding enthalpies of η^2-furan and η^2-DHF to both metals suggesting that this difference is the result of a partial loss of resonance energy in the case of the aromatic furan ligand upon interaction with the metal.

Introduction

The binding of metal centers across two carbons of aromatic systems is of considerable interest since such interactions can activate the organic ligand toward several chemical transformations including hydrogenation, electrophilic addition, and cycloaddition reactions.[1,2] Several instances are now known in which η^2 binding of π basic metals to aromatic systems results in complete dearomatization of the organic molecule. For example, the TpM(L)(π-acid) fragment [Tp = hydridotris(pyrazolyl)borate, M = rhenium, molybdenum, tungsten, L = variable ligand, π-acid = CO, NO] facilitates the dearomatization of several molecules including arenes, furans, pyrroles, and thiophenes.[2] Arene ligands can also bind in an η^2 fashion to relatively electron poor metal centers in fragments, such as $CpMn(CO)_2$ [Cp = η^5-C_5H_5] and $BzCr(CO)_2$ [Bz = η^6-C_6H_6]. However, in these cases the binding is quite weak primarily due to a reduced π interaction. Kinetic studies have provided an estimate of 11−15 kcal/mol for the strength of this weak metal−(η^2-arene) interaction.[3]

While several examples of stable, isolable, metal−(η^2-aromatic) complexes are known,[4] quantitative information regarding the strength of these interactions and the extent to which they disrupt the aromaticity of the coordinated ligand is rare. Such data is expected to be useful in obtaining a clearer understanding of this important interaction. We therefore report in this paper, a kinetic method to obtain an estimate of the strength of the [M]−(η^2-furan) and [M]−(η^2-DHF) interaction ([M] = $CpMn(CO)_2$, $BzCr(CO)_2$, DHF = 2,3-dihydrofuran]. Since the primary difference between furan and DHF is the aromatic character of the former molecule, a difference in the binding enthalpies of the two ligands is expected to provide an estimate for the disruption of the resonance stabilization of furan upon interaction with a metal center. Furthermore, since both Mn(I) and Cr(0) are d^6 metals, these experiments are expected to provide insight into the relationship between metal electron density and the binding energetics of the furan and DHF ligands. The high quantum yield for the photodissociation of a CO ligand from the parent tricarbonyls provides a convenient method for the generation of the [M]−(η^2-furan) and [M]−(η^2-DHF) complexes.[5] Since the reactivity of these molecules vary by several orders of magnitude, the displacement kinetics were studied from the nanosecond to the hours time scale using a variety of laser based time-resolved IR spectroscopic techniques. The relevant complexes were modeled using density functional theory to aid the interpretation of the experimental results and to better understand the metal−η^2 interaction.

*To whom correspondence should be addressed. E-mail: djdarens@mail.chem.tamu.edu (D.J.D.), ashfaq.bengali@qatar.tamu.edu (A.A.B.).

(1) (a) Harman, W. D.; Fairlie, D. P.; Taube, H. *J. Am. Chem. Soc.* **1986**, *108*, 8223. (b) Harman, W. D. *Chem. Rev.* **1997**, *97*, 1953.
(2) Keane, J. M.; Harman, W. D. *Organometallics* **2005**, *24*, 1786.
(3) (a) Bengali, A. A.; Grunbeck, A. *Organometallics* **2005**, *24*, 5919. (b) Bengali, A. A. *Organometallics* **2000**, *19*, 4000.
(4) For a comprehensive review see: Brooks, B. C.; Gunnoe, T. B.; Harman, W. D. *Coord. Chem. Rev.* **2000**, *206*, 3.
(5) Giordano, P. J.; Wrighton, M. S. *Inorg. Chem.* **1977**, *16*, 160.

Published on Web 07/20/2009

Experimental and Theoretical Methods

(a). Step-Scan and Rapid-Scan FTIR Studies. A Bruker Vertex 80 FTIR spectrometer equipped with both rapid and step-scan capabilities was used. Sample photolysis was conducted using 355 nm light from a Nd:YAG laser (50 mJ/pulse, 1 Hz repetition rate). To ensure a fresh solution was photolyzed by every laser shot, either a syringe or peristaltic pump was used to flow solution through a temperature controlled 0.5 mm path length IR cell with CaF_2 windows (Harrick Scientific). The temperature was monitored by a thermocouple located close to the photolysis solution and maintained by a water circulator to within ±0.1 °C. All spectra were obtained at 8 cm^{-1} resolution.

The photolysis solution contained ~4 mM $CpMn(CO)_3$ or $BzCr(CO)_3$ in cyclohexane solvent and was 0.53 M in either furan or DHF. To this solution varying amounts of pyridine was added as the displacing ligand. All kinetic runs were carried out under pseudo-first-order conditions with the concentration of pyridine at least ten times greater than that of [M]−(η^2-furan) and [M]−(η^2-DHF). The observed rate constants (k_{obs}) were obtained from single exponential fits to the absorbance versus time dependence of the reactant and product complexes. The reported errors were obtained from least-squares fits to the available data.

(b). Solution-Phase ATR-FTIR Studies. One hundred milligrams (0.490 mmol) of $CpMn(CO)_3$ was weighed into a vial and sealed with a septum in an argon-filled glovebox. The vial was moved into a fume hood and placed under an argon atmosphere where 10 mL of cyclohexane (CyH) was added via syringe. After dissolution, the $CpMn(CO)_3$ solution was cannulated to a jacketed reaction flask. The vial was rinsed with 10 mL of CyH, which was also cannulated into the reaction flask. After the addition of 1.0 mL (13.0 mmol) of DHF, a background scan was obtained. The reaction solution was then photolyzed with a 100 W Hg lamp (Newport) while it was monitored using an ASI ReactIR 1000 in situ FTIR until the $CpMn(CO)_3$ was consumed (~30 min). After the resulting $CpMn(CO)_2(\eta^2$-DHF) solution was heated to the desired temperature, the appropriate amount of CyH was added, and the temperature was allowed to stabilize (±0.5 °C). Upon addition of pyridine, a background was obtained and the reaction was monitored until the formation of $CpMn(CO)_2$(pyridine) was no longer observed.

(c). Synthesis of $CpMn(CO)_2(\eta^2$-DHF) and X-ray Crystal Analysis. One hundred milligrams (0.49 mmol) of $CpMn(CO)_3$ was weighed into a 50 mL round-bottom flask with a Teflon coated stir bar in an argon filled glovebox and sealed with a septum. The complex was dissolved in 20 mL of CyH, and 1 mL (13.0 mmol) of DHF was added. The solution was photolyzed for approximately 2 h, after which solvent was removed via vacuum. Crystals suitable for X-ray analysis were obtained from slow evaporation of a diethyl ether solution of the complex in the presence of pentane and selected using a Lecia microscope. The representative crystal was coated with cryogenic protectant and affixed to a nylon sample loop. The crystal was placed in a cold nitrogen stream and maintained at 213 K. Data was collected on a Bruker-AXS ApexII diffractometer and covered more than a hemisphere of reciprocal space. The structure was solved using direct methods utilizing SAINT,[6] SHELX,[7] and XSEED[8] suite of programs. Crystal details and details of data collection can be found in the Supporting Information.

(d). Nanosecond IR studies. The laser-based TRIR apparatus at the Nottingham University is based upon the PIRATE facility at the Rutherford Appleton Laboratory[9] and has been described previously.[10] Briefly, a commercial Ti:sapphire oscillator (MaiTai)/regenerative amplifier system (Spitfire Pro, Spectra Physics, 1kHz) is used to generate 800 nm laser pulses which pumps a TOPAS-C OPA (Light Conversion) with a DFG (difference frequency generator) unit to produce a tunable mid-IR pulse with a spectral bandwidth of ~180 cm^{-1}. Part of the IR pulse is reflected onto a single-element MCT detector (Kolmar Technology) to serve as a reference, and the other part serves as the probe beam, which is focused and overlaps with the pump beam at the sample position.

In these experiments on the nanosecond/microsecond time scale the excitation pulse from a Q-switched Nd:YVO laser (ACE- 25QSPXHP/MOPA, Advanced Optical Technology, UK) is synchronized to the Spitfire Pro amplifier. The delay between pump and probe pulses can be controlled with a pulse generator (DG535, Stanford Research System) from 0.5 ns to 100 μs. The broadband transmitted probe pulse is detected with a HgCdTe array detector (Infrared Associates), which consists of 128 elements, amplified by a 144-channel amplifier and digitized by a 16-bit analogue-to-digital converter (IR-0144, Infrared Systems Development Corp.). The measurements were performed on flowing solutions (3 mmol) in a CaF_2 IR cell, which was also raster-scanned to prevent localized laser-heating and photochemical decomposition.

(e). DFT Calculations. The aromatic stabilization energy for furan was calculated through an extrapolation of the energy of hydrogenation of DHF and furan. This hydrogenation energy was calculated using the meta-GGA density functional of Tao, Perdew, Staroverov, and Scuseria[11] (TPSS) with the aug-cc-pvTz[12] basis set at the optimum geometries.

For the ligated metal complexes, TPSS was also used as it has been shown to perform well for transition metal systems. In order to keep computational costs low, geometry optimization and frequency calculations were done using the Couty-Hall[13] basis set as in the previous work on this type of system.[14] All enthalpies of binding were thus calculated as the differences of the TPSS/aug-cc-pvTz energies plus frequency corrections from TPSS/Couty-Hall.

All calculations were performed in the development version of the GAUSSIAN suite of programs[15] using the high-performance

(6) *SAINT-Plus*, version 6.02; Bruker: Madison, WI, **1999**.
(7) (a) Sheldrick, G. *SHELXS-86: Program for Crystal Sructure Solution*; Institut fur Anorganische Chemie der Universitat: Gottingen, Germany, **1986**. (b) Sheldrick, G. *SHELXS-97: Program for Crystal Structure Refinement*; Institut fur Anorganische Chemie der Universitat: Gottingen, Germany, **1997**. (c) *SHELXTL*, version 5.0; Bruker: Madison, WI, **1999**.
(8) Barbour, L. J. *J. Supramol. Chem.* **2001**, *1*, 189.
(9) Towrie, M.; Grills, D. C.; Dyer, J.; Weinstein, J. A.; Matousek, P.; Barton, R.; Bailey, P. D.; Subramaniam, N.; Kwok, W. M.; Ma, C. S.; Phillips, D.; Parker, A. W.; George, M. W. *Appl. Spectrosc.* **2003**, *57*, 367.
(10) Brennan, P.; George, M. W.; Jina, O. S.; Long, C.; McKenna, J.; Pryce, M. T.; Sun, X. Z.; Vuong, K. Q. *Organometallics* **2008**, *27*, 3671.
(11) Tao, J. M.; Perdew, J. P.; Staroverov, V. N.; Scuseria, G. E. *Phys. Rev. Lett.* **2003**, *91*, 146401.
(12) Kendall, R. A.; Dunning, T. H.; Harrison, R. J. *J. Chem. Phys.* **1992**, *96*, 6796.
(13) Couty, M.; Hall, M. B. *J. Comput. Chem.* **1996**, *17*, 1359.
(14) Bengali, A. A.; Hall, M. B.; Wu, H. *Organometallics* **2008**, *27*, 5826.
(15) M. Frisch, J.; Trucks G. W.; Schlegel, H. B.; Scuseria, G. E.; Robb, M. A.; Cheeseman, J. R.; Montgomery, Jr. J. A.; Vreven, T.; Scalmani, G.; Mennucci, B.; Barone, V.; Petersson, G. A.; Caricato, M.; Nakatsuji, H.; Hada, M.; Ehara, M.; Toyota, K.; Fukuda, R.; Hasegawa, J.; Ishida, M.; Nakajima, T.; Honda, Y.; Kitao, O.; Nakai, H.; Li, X., Hratchian, H. P., Peralta, J. E.; Izmaylov, A. F.; Kudin, K. N.; Heyd, J. J.; Brothers, E.; Staroverov, V. N.; Zheng, G.; Kobayashi, R.; Normand, J.; Sonnenberg, J. L.; Ogliaro, F.; Bearpark, M.; Parandekar, P. V.; Ferguson, G. A.; Mayhall, N. J.; Iyengar, S. S.; Tomasi, J.; Cossi, M.; Rega, N.; Burant, J. C.; Millam, J. M.; Klene, M.; Knox, J. E.; Cross, J. B.; Bakken, V.; Adamo, C.; Jaramillo, J.; Gomperts, R.; Stratmann, R. E.; Yazyev, O.; Austin, A. J.; Cammi, R.; Pomelli, C.; Ochterski, J. W.; Ayala, P. Y.; Morokuma, K.; Voth, G. A.; Salvador, P.; Dannenberg, J. J.; Zakrzewski, V. G.; Dapprich, S.; Daniels, A. D.; Strain, M. C.; Farkas, O.; Malick, D. K.; Rabuck, A. D.; Raghavachari, K.; Foresman, J. B.; Ortiz, J. V.; Cui, Q.; Baboul, A. G.; Clifford, S.; Cioslowski, J.; Stefanov, B. B.; Liu, G.; Liashenko, A.; Piskorz, P.; Komaromi, I.; Martin, R. L.; Fox, D. J.; Keith, T.; Al-Laham, M. A.; Peng, C. Y.; Nanayakkara, A.; Challacombe, M.; Chen, W.; Wong, M. W.; Pople, J. A. *Gaussian Development Version*, revision G.03; Gaussian Inc., Wallingford, CT, **2008**.

Scheme 1

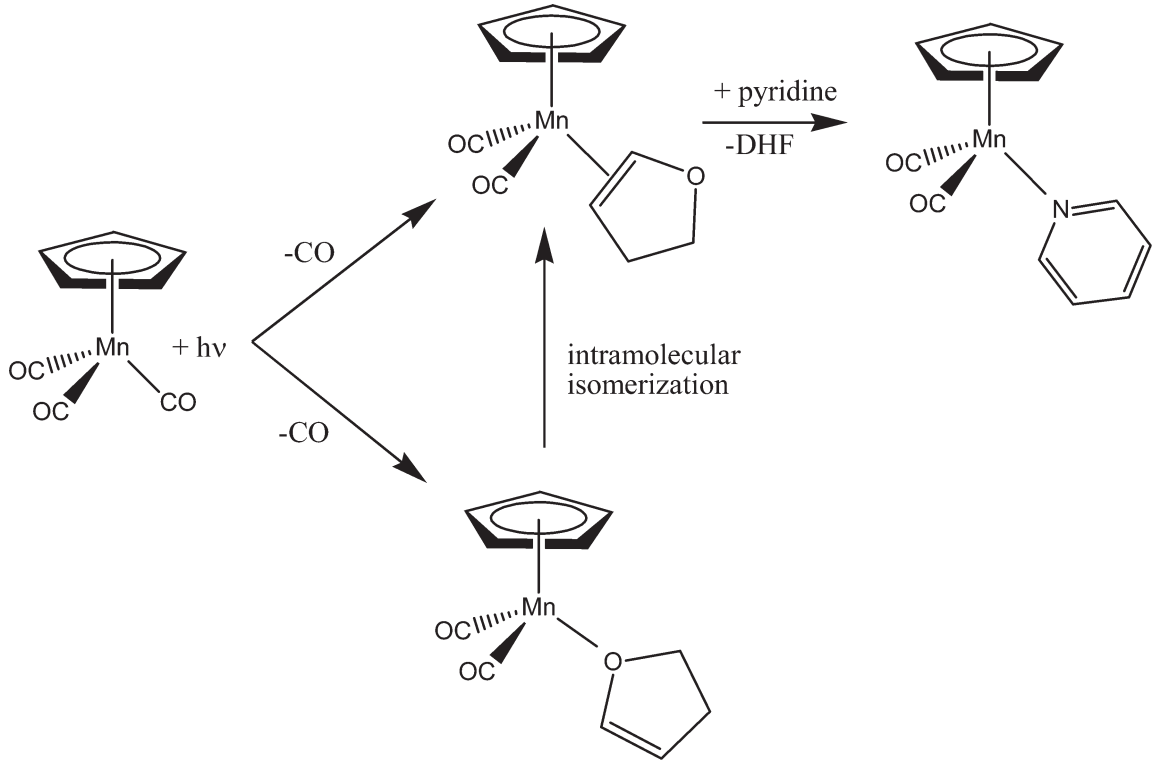

computing facilities available at Texas A&M University at Qatar.

Results and Discussion

(a). 2,3-DHF. As previously reported, photolysis of a cyclohexane solution of $CpMn(CO)_3$ or $BzCr(CO)_3$ in the presence of DHF results in the formation of the linkage isomers [M]−(η^1-O-DHF) and [M]−(η^2-C,C-DHF).[14] The oxygen-bound isomer converts to the more stable η^2 isomer on the millisecond and microsecond time scales for the Mn and Cr complexes, respectively. In the present study, the subsequent displacement of the η^2-bound DHF ligand from the metal center by pyridine was followed by FTIR spectroscopy (Scheme 1). Since the reactivity of the [M]−(η^2-DHF) complexes was significantly different for the two metal centers, rapid-scan FTIR and solution-phase ATR techniques were utilized in the case of the Cr and Mn complexes, respectively.

As shown in Figure 1, in the presence of 0.06 M pyridine, the Cr-(η^2-DHF) complex with CO stretching absorbances at 1924 and 1869 cm^{-1} undergoes a first-order exponential decay at the same rate at which the previously observed $BzCr(CO)_2$(pyridine) complex (1897 and 1847 cm^{-1}) grows.[16] Similar spectral behavior was observed in the case of the Mn complex with the Mn-(η^2-DHF) complex absorbing at 1968 and 1906 cm^{-1} reacting with pyridine to form the $CpMn(CO)_2$(pyridine) complex with CO bands at 1932 and 1866 cm^{-1}.[5] The two metal systems showed remarkably different reactivity, however. Under similar conditions of temperature and [pyridine], the Cr-(η^2-DHF) complex reacted with pyridine almost 50 000 times faster than the analogous Mn complex. As discussed below, this difference in reactivity is related to a stronger interaction between the DHF ligand and the Mn center.

As shown in Figure 2, k_{obs} exhibits a nonlinear dependence on [pyridine] at all temperatures and approaches a limiting value at high [pyridine] for both metals. This saturation behavior is consistent with a dissociative mechanism for the substitution reaction (Scheme 2). The displacement of other weakly coordinated solvents, such as arenes, alkenes, THF, and silanes, from the $CpMn(CO)_2$ and $BzCr(CO)_2$ fragment have also been shown to proceed by a dissociative pathway.[3,17] Since this reaction proceeds in cyclohexane solvent, the [M]−CyH complex is shown as an intermediate since it has previously been observed on the microsecond time scale.[18,19] Assuming a steady state concentration of the [M]−CyH intermediate, the dependence of k_{obs} on [pyridine] can be derived as

$$k_{obs} = \frac{k_1 k_2[\text{pyridine}]}{k_{-1}[\text{DHF}] + k_2[\text{pyridine}]} \qquad (1)$$

A fit of the data shown in Figure 2 according to eq 1, yields values of k_1 and k_2/k_{-1} for the displacement reaction. As shown in Table 1, at 323K the value of k_1, the rate constant associated with the breaking of the [M]−(η^2-DHF) bond, is almost 50 000 times larger in the case of Cr than Mn. An Eyring analysis indicates that this difference

(16) Strohmier, W.; Hellmann, H. *Chem. Ber.* **1963**, *96*, 2859.

(17) (a) Bengali, A. A.; Fehnel, R. *Organometallics* **2005**, *24*, 1156. (b) Cole, S.; Dulaney, K. E.; Bengali, A. A. *J. Organomet. Chem.* **1998**, *55*, 560. (c) Hester, D. M.; Sun, J.; Harper, A. W.; Yang, G. K. *J. Am. Chem. Soc.* **1992**, *114*, 5234.

(18) (a) Cowan, A. J.; George, M. W. *Coord. Chem. Rev.* **2008**, *252*, 2504.

(19) Lugovskoy, S.; Lin, J.; Schultz, R. H. *Dalton Trans.* **2003**, 3103.

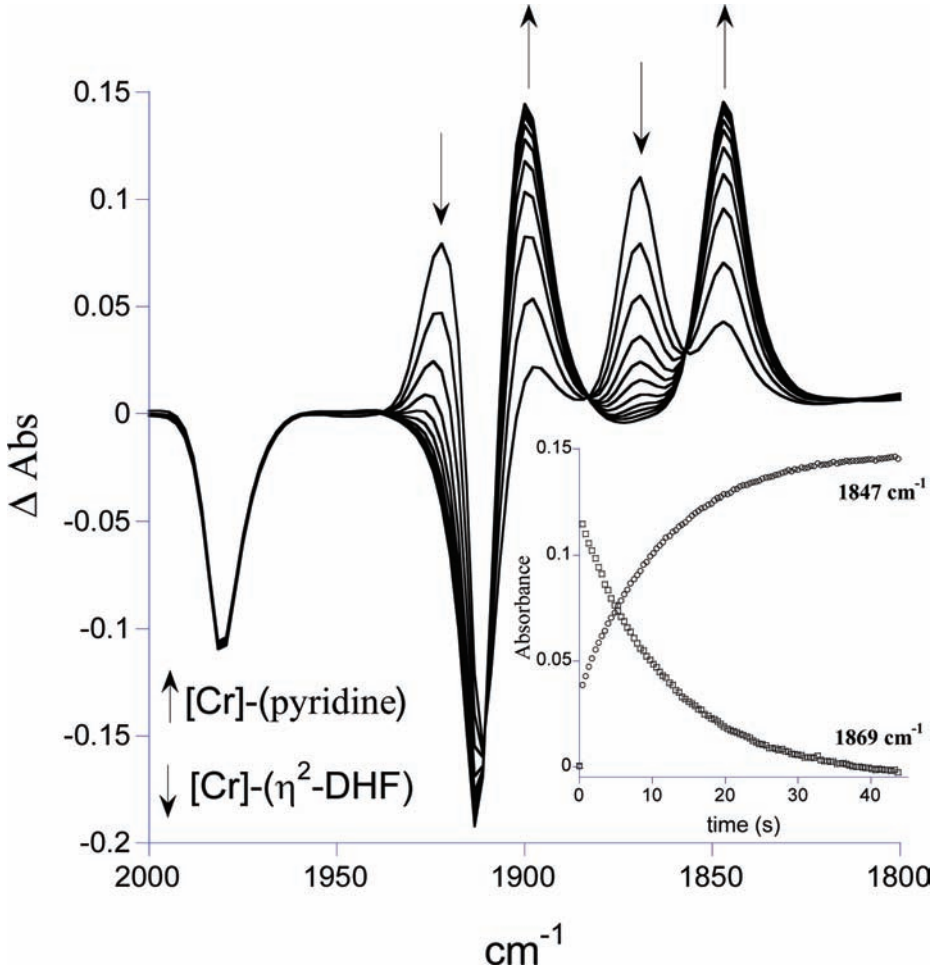

Figure 1. Difference absorbance spectra showing the reaction of the photolytically generated $BzCr(CO)_2(\eta^2\text{-DHF})$ complex with 0.06 M pyridine at 293 K. The spectra were obtained at 4s intervals. The decay and growth of the reactant and product complexes are shown in the inset.

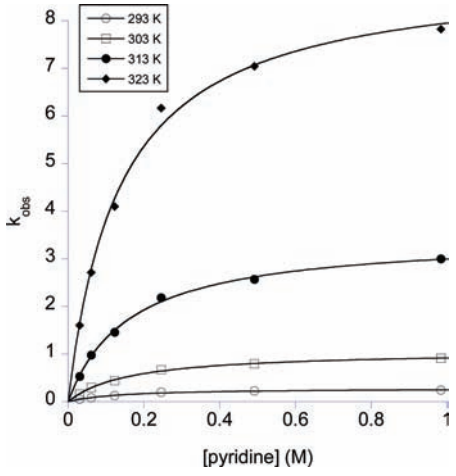

Figure 2. A plot of k_{obs} vs [pyridine] at several temperatures for the reaction of [Cr]-(η^2-DHF) with pyridine. The pyridine concentration was varied from ~0.03 to 1 M The saturation behavior of k_{obs} at high [pyridine] is consistent with a dissociative mechanism for the substitution of the DHF ligand.

in the rate constant is primarily caused by a ~ 7 kcal/mol larger activation enthalpy in the case of the Mn complex. The large positive activation entropies of +11−12 e.u associated with k_1 are consistent with the dissociation of the [M]−(η^2-DHF) bond in the transition state. Assuming

Scheme 2

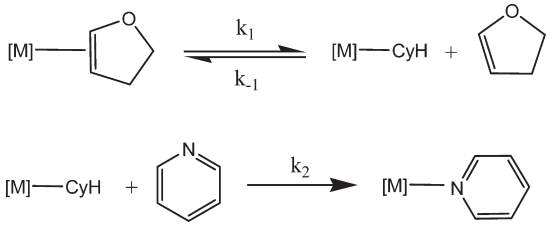

Table 1. Rate Constants and Activation Parameters Obtained from Fits to the k_{obs} vs [Pyridine] Data According to eq 1 for the Reaction: [M]−(η^2-DHF) + pyridine → [M]−pyridine + DHF

[M] = $CpMn(CO)_2$			[M] = $BzCr(CO)_2$		
T (K)	k_1 (s^{-1}) ×10^4	k_2/k_{-1}	T (K)	k_1 (s^{-1})	k_2/k_{-1}
323	1.9 ± 0.2	3.0 ± 1.2	293	0.29 ± 0.01	3.7 ± 0.5
333	7.0 ± 0.5	4.8 ± 1.4	303	1.1 ± 0.1	3.3 ± 0.2
343	22 ± 1	5.7 ± 1.0	313	3.5 ± 0.1	3.3 ± 0.2
353	93 ± 5	4.2 ± 1.0	323	9.0 ± 0.3	3.9 ± 0.4
$\Delta H_1^{\ddagger}$ = 28 ± 1 kcal/mol $\Delta S_1^{\ddagger}$ = +12 ± 4 e.u			$\Delta H_1^{\ddagger}$ = 21 ± 1 kcal/mol $\Delta S_1^{\ddagger}$ = +11 ± 2 e.u		

that the CyH solvent coordinates to the metal center after dissociation of the DHF molecule in the transition state, activation enthalpies of 21 ± 1 and 28 ± 1 kcal/mol for the Cr and Mn complexes, respectively, are expected to

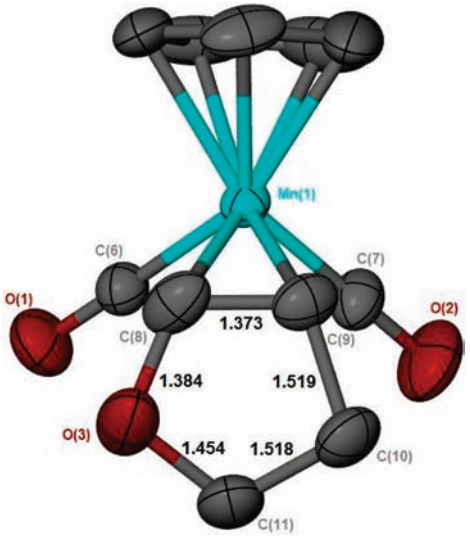

Figure 3. Molecular structure of the $CpMn(CO)_2(\eta^2$-DHF) complex.

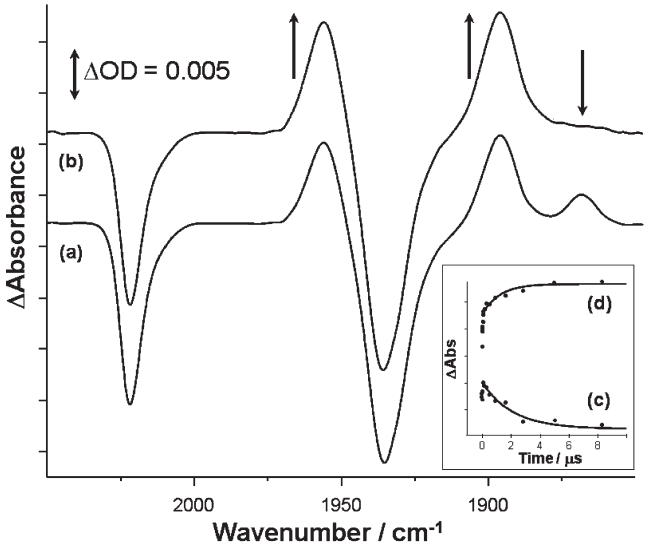

Figure 4. TRIR difference absorbance spectra showing the reaction of the photolytically generated $CpMn(CO)_2(\eta^2$-furan) complex at 298 K obtained at (a) 1 ns and (b) 10 μs after photolysis. The decay and growth of the bands at (c) 1869 and (d) 1956 cm^{-1} are shown in the inset.

provide reliable estimates for the strength of the [M]−(η^2-DHF) interaction.

The agreement between the experimental activation enthalpies and the calculated bond dissociation enthalpies (BDEs) discussed later, suggest that the [M]−(η^2-DHF) bond is mostly broken in the transition state. The weaker binding of DHF to the Cr center is consistent with previous studies that have also demonstrated a weaker interaction between the $BzCr(CO)_2$ fragment and ligands such as THF and η^2 coordinated arenes relative to $CpMn(CO)_2$.[3,17] The lower ν_{CO} band positions suggests that $BzCr(CO)_2$ fragment is more electron rich than $CpMn(CO)_2$ and the difference in the binding strengths may the result of a reduction in L → metal σ donation in the former metal system.

Values of the k_2/k_{-1} ratios obtained from fits to the k_{obs} versus [pyridine] data according to eq 1 indicate that the intermediate [M]−CyH complex is not very selective in its reaction with either DHF or pyridine. The k_2/k_{-1} ratios range from 3 to 6 and are relatively insensitive to temperature indicating that the enthalpic barriers for the reaction of [M]−CyH with either DHF or pyridine are similar. This observation is consistent with the results of previous studies that have focused on investigating the reactivity of the [M]−CyH solvate complex. For example, $CpMn(CO)_2$(CyH) was observed to react 3−4 times faster with pyrrolidine than with cyclopentene with only a 1.6 kcal/mol difference in the activation enthalpies.[19]

The relatively large binding enthalpy for the [Mn]−(η^2-DHF) complex allowed us to successfully isolate this species. The crystal structure for the $CpMn(CO)_2(\eta^2$-DHF) complex is shown in Figure 3. The metal is bound almost symmetrically to a π face of the η^2 coordinated ligand with Mn−C(8) and Mn−C(9) bond distances of 2.203(2) Å and 2.171(2) Å, respectively. Importantly, the coordinated C=C bond length of 1.373 Å is greater than a typical length of 1.33 Å for an uncoordinated double bond. While some lengthening is expected because of conjugation with the oxygen atom, results of the DFT calculations discussed later suggest that the relatively long C=C bond length is indicative of a π backbonding interaction with the metal which serves to weaken the C=C bond.

(b). Furan. Photolysis of either parent tricarbonyl in the presence of furan generates a single dicarbonyl complex with CO stretching absorptions at 1869, 1925 cm^{-1} and 1906, 1965 cm^{-1} for the Cr and Mn complexes, respectively. By analogy with the CO stretching bands of the [M]−(η^2-DHF) complex and also $CpMn(CO)_2(\eta^2$-cyclopentene),[19] this species is assigned as the [M]−(η^2-furan) complex. Interestingly, unlike DHF, there is no evidence for the presence of the oxygen bound [Mn]−(η^1-O-furan) linkage isomer on the millisecond time scale, although as shown in Figure 4, experiments done on the submicrosecond time scale in neat furan provide evidence for the formation of this complex absorbing at 1869 cm^{-1}.

At 298 K, this species has a half-life of ~2 μs converting to the more stable [Mn]−(η^2-furan) complex. The conversion of the η^1-O to the η^2-(C,C) isomer is almost 3000 times faster in the case of furan relative to DHF suggestive of a lower enthalpic barrier (~2−3 kcal/mol) for the isomerization reaction. The weaker η^1-O binding of furan suggests that the oxygen lone pairs are not easily available for binding to the metal center presumably because of delocalization within the aromatic ring system. Alternatively, the available lone pair on the oxygen atom in furan may be held tighter because of greater *s* character resulting in weaker donor characteristics for this ligand.

In the presence of pyridine, [M]−(η^2-furan) converts to the [M]−pyridine complex more than 20 000 times faster than in the case of the analogous [M]−(η^2-DHF) system. The saturation behavior of k_{obs} shown in Figure 5 indicates that, like DHF, the displacement of η^2 coordinated furan by pyridine follows a dissociative pathway. The displacement of furan from the Cr center also proceeds more than 10 000 times faster than from the Mn center indicative of a weaker binding of furan in the former case. Values of k_1 and k_2/k_{-1} obtained from a fit to the k_{obs} versus [pyridine] data are presented in Table 2. From the temperature dependence of k_1, activation enthalpies of 22 ± 1 kcal/mol and ~11 kcal/mol are obtained for the dissociation of the Mn−(η^2-furan) and

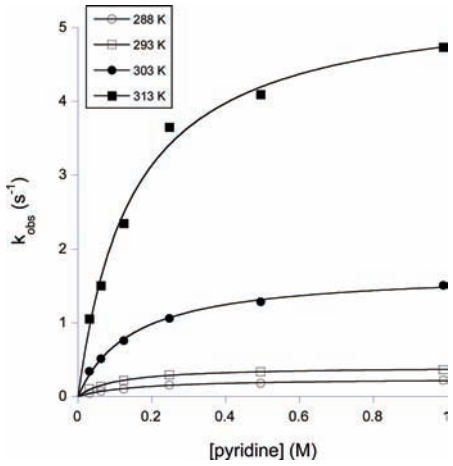

Figure 5. Plot of k_{obs} vs [pyridine] at several temperatures for the reaction of $CpMn(CO)_2$-(η^2-furan) with pyridine. The saturation behavior of k_{obs} at high [pyridine] is consistent with a dissociative mechanism for the substitution of the furan ligand.

Table 2. Rate Constants and Activation Parameters Obtained from Fits to the k_{obs} vs [Pyridine] Data According to eq 1 for the Reaction: [M]−(η^2-furan) + pyridine → [M]−pyridine + furan

$CpMn(CO)_2$			$BzCr(CO)_2$		
T (K)	k_1 (s^{-1})	k_2/k_{-1}	T (K)	k_1 (s^{-1}) × 10^{-3}	k_2/k_{-1}
288	0.25 ± 0.01	3.5 ± 0.4	293	5.8 ± 0.6	2.0 ± 0.3
293	0.41 ± 0.01	5.3 ± 0.5	305	12 ± 1	3.2 ± 0.3
303	1.7 ± 0.1	3.8 ± 0.3			
313	5.4 ± 0.2	3.7 ± 0.5			
$\Delta H_1^{\ddagger} = 22 \pm 1$ kcal/mol			$\Delta H_1^{\ddagger} \approx 11$ kcal/mol		
$\Delta S_1^{\ddagger} = +15 \pm 3$ e.u			$\Delta S_1^{\ddagger} \approx 0$ e.u		

Cr−(η^2-furan) bonds. Both $\Delta H_1^{\ddagger}$ and $\Delta S_1^{\ddagger}$ in the case of the Cr system are expected to be estimates since k_1 was only determined at two temperatures over a narrow range ($\Delta T = 12$ K).[20]

As shown in Table 3, estimates for the bond dissociation enthalpies of the [M]−(η^2-DHF) and [M]−(η^2-furan) complexes show that both furan and DHF bind to Cr ~7−11 kcal/mol weaker than to the Mn center. Interestingly, there is also a 6−10 kcal/mol difference in binding between [M]−(η^2-DHF) and [M]−(η^2-furan). Since the primary difference between furan and DHF is that the former ligand is aromatic, the 6−10 kcal/mol difference in the bond strengths can be related to the disruption of the resonance stabilization of the furan ligand upon binding to the metal. A [M] → L π backbonding interaction would serve to localize electron density about the carbons bound to the metal center, resulting in partial loss of resonance energy in the case of the aromatic furan molecule.

(20) Because of the significantly faster displacement rate, step-scan FTIR was used to study the kinetics of substitution in $BzCr(CO)_2$(η^2-furan). The experimental conditions therefore required a continuous flow of the photolysis solution through the IR cell. Because of the low boiling point of furan, the maximum temperature at which the thermostatted photolysis solution could be held was 40 °C. Because of thermal losses in the delivery tubing, the solution temperature dropped to 32 °C at the cell, and this was therefore the maximum temperature at which the reaction could be studied. Difficulties with moisture condensation on the cell windows prevented temperatures lower than 20 °C from being utilized. These experimental difficulties were not experienced in the case of the Mn system since the reaction was slow enough to use rapid-scan FTIR, which did not require a continuous flow of solution.

Table 3. Experimental and Theoretical Estimates for the BDE's of the [M]−(η^2-furan) and [M]−(η^2-DHF) Interactions[a]

complex	ΔH_1 (kcal mol^{-1})
[Mn]−(η^2-DHF)	28 (29.2)
[Mn]−(η^2-furan)	22 (20.6)
[Cr]−(η^2-DHF)	21 (21.3)
[Cr]−(η^2-furan)	~11 (14.1)

[a] Numbers in parentheses were obtained from DFT calculations at the TPSS/aug-cc-pTZ level of theory.

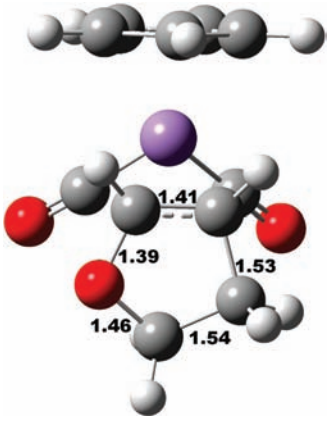

Figure 6. Calculated structure of the $CpMn(CO)_2$(η^2-DHF) complex.

Table 4. Calculated and Experimental Bond Distances[a]

	bond distance (Å)		
molecule	C(8)−C(9)	[M]−C(8)	[M]−C(9)
furan	1.37		
DHF	1.34		
[Mn]−(η^2-DHF)	1.41	2.21	2.16
[Mn]−(η^2-DHF)b	1.379	2.203	2.171
[Mn]−(η^2-furan)	1.42	2.19	2.26
[Cr]−(η^2-DHF)	1.40	2.34	2.26
[Cr]−(η^2-furan)	1.41	2.31	2.39

[a] Numbering scheme refers to Figure 3. [b] Experimental values.

The binding enthalpy difference can then be attributed to the energetic cost of disrupting the aromaticity of the furan ligand upon coordination to the $CpMn(CO)_2$ or $BzCr(CO)_2$ fragment. These results therefore provide important *quantitative* information about the capability of the metal center to dearomatize the dihapto coordinated ligand. In an effort to better understand the bonding interaction between the metal centers and the DHF and furan ligands, DFT calculations were performed to lend support for the experimental findings.

Calculations

The calculated structure of the [Mn]−(η^2-DHF) complex is shown in Figure 6, and the relevant structural parameters for all the complexes and the calculated BDE's are shown in Tables 4 and 3, respectively. Comparison of the $CpMn(CO)_2$-(η^2-DHF) structures in Figures 3 and 6 and the structural parameters shown in Table 4 demonstrate good agreement between the calculated and experimental values. The calculated BDE's are also in excellent agreement with the experimentally determined numbers suggesting that the activation

Scheme 3

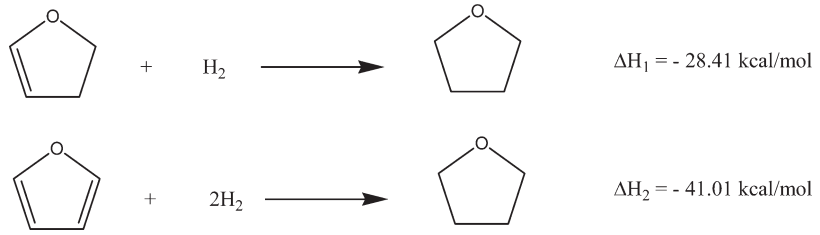

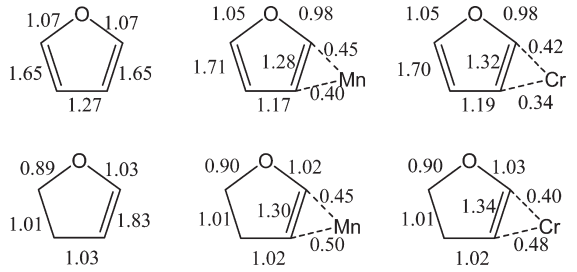

Figure 7. Calculated bond orders for uncoordinated and coordinated furan and DHF ligands.

enthalpies provide reliable estimates for the M−L bond strengths. This agreement provides further support for the conclusion that the substitution reaction proceeds through a dissociative mechanism and that the M−L bond is fully dissociated in the transition state.

The distances between the metal and the carbon atoms of the coordinated π bond are ~0.1 Å shorter in the [Mn]−(η^2-DHF) and [Mn]−(η^2-furan) complexes relative to the analogous Cr system, consistent with a weaker binding of both ligands to Cr. For both metals, the coordinated C=C bond distances are ~4−5% greater than in free DHF and furan. This increase in the C=C bond distance upon binding is suggestive of a π backbonding contribution to the overall metal−η^2 interaction. Again, in agreement with the experimental and theoretical findings of a stronger interaction with the DHF ligand for both metal centers, the [M]−(η^2-DHF) bond length is slightly less than that of [M]−(η^2-furan).

Among the heterocycles, furan, thiophene, and pyrrole, furan is considered to be the least aromatic because of the higher electronegativity of the oxygen atom. Various estimates have placed the aromatic stabilization of furan in the range of 11−23 kcal/mol.[21,22] We obtained an estimate for the resonance stabilization of the furan ligand by calculating the enthalpy of the hydrogenation reactions shown in Scheme 3. The aromatic stabilization of furan was calculated as $\Delta H_2 - 2\Delta H_1$ yielding a value of 15.8 kcal/mol and falls in the range of values mentioned above. The observed 6−10 kcal/mol difference in the binding of furan to the BzCr(CO)$_2$ and CpMn(CO)$_2$ fragments relative to DHF, may then be related to a ~50% loss in the resonance stabilization of the aromatic ligand.

A natural bond order analysis (NBO) was performed to provide insight into the interaction of furan and DHF with the Cr and Mn centers. As shown in Figure 7, the bond orders for free furan show some degree of delocalization of the π system with a C−C bond order of 1.27. The reduction in both the C−C and C=C bond orders upon binding is suggestive of a localization of electron density about the metal−η^2 bond and a disruption of the π system of the aromatic ligand. Upon binding to either the Cr or Mn center, the order of the coordinated π bond decreases by 20% and 30% for furan and DHF, respectively. This observation suggests that the extent of the π backbonding contribution is independent of the metal and that therefore the weaker binding of furan and DHF to Cr relative to Mn is likely the result of reduced L → M σ donation in the case of the more electron rich BzCr(CO)$_2$ fragment. The NBO analysis also suggests that the reduction in the C=C bond order is less in the case of furan indicating a reduced contribution of π backbonding in furan relative to DHF. This conclusion is not surprising since the π interaction is expected to be energetically unfavorable due to loss of resonance energy in the case of the aromatic furan ligand.

Conclusions

Photolysis of CpMn(CO)$_3$ and BzCr(CO)$_3$ in the presence of furan or DHF results in the formation of the respective metal−η^2 bound complexes. The displacement of the dihapto bound ligand by pyridine was studied using several different FTIR techniques. The substitution reaction follows a dissociative pathway and the temperature dependence of the limiting rate constant provides an estimate for the strength of the metal−η^2 interaction. The results suggest that both DHF and furan bind ~7−11 kcal/mol weaker to the Cr center than to Mn. This difference in binding enthalpy is presumably because of the reduced L → M σ donation in the case of the more electron rich BzCr(CO)$_2$ fragment. Interestingly, for both metal systems, the interaction between the metal and the DHF ligand is stronger (~6−10 kcal mol^{-1}) than with furan. This difference in binding enthalpy is attributed to a partial loss of resonance energy in the case of the aromatic furan molecule. Theoretical calculations employing DFT are consistent with this conclusion. Further studies aimed at investigating the effect of varying the electronic environment of the metal centers upon the binding energetics are currently under way.

Acknowledgment. This research was supported by a National Priorities Research Program (NPRP) grant from the Qatar National Research Fund (Grant 8-6-7-1). M.W.G. gratefully acknowledges receipt of a Royal Society Wolfson Merit Award.

Supporting Information Available: Details of the CpMn(CO)$_2$(η^2-DHF) crystal structure and data collection. This material is available free of charge via the Internet at http://pubs.acs.org.

(21) Epiotis, N. D.; Cherry, W. R.; Bernardi, W. R.; Hehre, W. J. *J. Am. Chem. Soc.* **1976**, *98*, 4361.
(22) Bean, G. P. *J. Org. Chem.* **1998**, *63*, 2497.